PAPER • **OPEN ACCESS**

Theoretical study of single ionization of the oxygen atom

To cite this article: V Jonauskas 2025 *Phys. Scr.* **100** 075403

Physica Scripta

PAPER

Theoretical study of single ionization of the oxygen atom

V Jonauskas
Institute of Theoretical Physics and Astronomy Vilnius University, Saulėtekio av. 3 LT-10257 Vilnius, Lithuania
E-mail: valdas.jonauskas@tfai.vu.lt

Keywords: atomic data, ionization, oxygen

OPEN ACCESS

RECEIVED
3 March 2025

REVISED
13 May 2025

ACCEPTED FOR PUBLICATION
3 June 2025

PUBLISHED
13 June 2025

Abstract

Understanding electron-impact ionization of oxygen is crucial because of its abundance and key role in influencing plasma dynamics in both cosmic and laboratory environments. This work examines the single ionization from energy levels of the ground configuration of atomic oxygen. The direct ionization (DI) and excitation-autoionization (EA) processes are examined for the 2*s* and 2*p* subshells of the ground configuration. The scaled distorted wave (sDW) cross sections, calculated using the experimental ionization threshold, show a good agreement with measurements. Additionally, the sDW results closely follow those obtained using the binary encounter Bethe model. A comparison of the DI 2*s* and 2*p* cross sections, previously calculated using the B-spline R-matrix-with-pseudostates (BSR) method, to the sDW data reveals similar peak values, except for the $^1S_0$ level, where the BSR calculations predict ∼15% higher contribution for the DI 2*p* channel relative to the sDW data. For the EA process, the sDW cross sections exceed the BSR calculations by approximately a factor of two. For spin-forbidden transitions, $2p^4\ ^3P \rightarrow 2p^3 3s\ ^5S$ and $2p^4\ ^3P \rightarrow 2p^3 3p\ ^5P$, the sDW cross sections are slightly lower than those predicted by the BSR method. These findings highlight reliability of the sDW method for oxygen ionization modeling and suggest correlation effects may explain discrepancies with BSR.

1. Introduction

Oxygen, as one of the most abundant elements in the universe, plays an important role in the physical and chemical processes that shape the evolution of cosmic systems [1–5]. Oxygen is often present as a component of low-temperature and high-temperature plasmas, such as those found in fusion research [6, 7], electric arc discharges [8], and plasma processing [9].

To accurately model and predict plasma behavior, we must have reliable data on ionization and recombination rates, as these processes influence motion and distribution of charged particles. These processes play a key role in determining the accuracy of transport models and the resulting emission power spectrum predictions. By thoroughly understanding and accurately representing atomic collisions, we can gain deeper insights into the behavior of oxygen under different plasma conditions.

Purpose of the this paper is to study electron-impact single ionization cross sections from energy levels of the ground configuration of the oxygen atom. The scaled distorted wave (sDW) approximation [10–12] is employed to determine contribution of the direct and indirect ionization processes. Excitations from the ground configuration with subsequent autoionization are analyzed for the indirect process. A detailed comparison with previous calculations [13–15] and experimental data [16–18] is provided.

Previously, the crossed-beams approach was implemented to obtain ionization cross sections for the O atom [19, 20]. The absolute crossed-beams method using a fast atom beam was applied by Brook *et al* [16]. Zipf [17] presented the experimental ionization cross sections from 40 to 300 eV. These results were normalized in the 100–300 eV energy range to fit data from Fite and Brackman [19] and Brook *et al* [16]. Later, the electron-impact ionization for the oxygen atom was examined using a pulsed crossed beam technique incorporating time-of-flight spectroscopy by Thompson *et al* [18]. Their results were normalized to the higher energy values of Brook *et al* [16].

Single ionization cross sections were previously calculated using binary encounter Bethe (BEB) model [13], momentum-space coupled-channels-optical (CCO) [14], and B-spline R-matrix-with-pseudostates (BSR) approaches [15]. Good agreement with measurements was demonstrated in these calculations. However, the CCO and BSR data were presented up to 300 eV and 200 eV, respectively.

In the next section, we describe the theoretical methods used in this paper. Section 3 then presents our results, and in section 4, we summarize the work.

2. Theoretical approach

Cross sections for electron-impact single ionization of the O atom have been investigated using the Dirac-Fock-Slater (DFS) aproximation implemented in Flexible atomic code (FAC) [21]. Direct ionization (DI),

$$e^- + \mathrm{O} \rightarrow \mathrm{O}^+ + e^- + e^-, \tag{1}$$

and excitation autoionization (EA), which is a two-step process,

$$e^- + \mathrm{O} \rightarrow \mathrm{O}^* \rightarrow \mathrm{O}^+ + e^- + e^-, \tag{2}$$

are independently estimated. Here, O^* represents excited autoionizing states of the atom. The excited autoionizing states can decay through Auger and radiative transitions [11]. The radiative decay reduces the population transferred to the states of the O^+ ion. FAC [21] is used here to calculate the radiative and Auger transition probabilities.

Excited autoionizing states of the oxygen atom can be reached through the dielectronic capture when negative ion of oxygen is formed. However, contribution from the dielectronic capture followed by double autoionization to the single ionization is often much smaller compared to the DI and EA processes and, therefore, are not considered in this work. The same can be said about the simultaneous ionization-excitation process [22].

The distorted wave (DW) excitation cross sections from initial level i to the final level f are given by [21]:

$$\sigma_{if}(\epsilon_i) = \frac{2\pi}{k_i^2[J_i]} \sum_{j_i j_f} \sum_{J} [J] \left| \left\langle K_f \gamma_f J_f \ \epsilon_f j_f \ JM \right| \sum_{p<q} \frac{1}{r_{pq}} \left| K_i \gamma_i J_i \ \epsilon_i j_i JM \right\rangle \right|^2, \tag{3}$$

where k_i is the kinetic momentum of the incident electron, K_i (K_f) is the initial (final) configuration, γ is multielectron quantum numbers of the configuration, J_i (J_f) is the total angular momentum quantum number of the initial (final) configuration, $\epsilon_i j_i$ ($\epsilon_f j_f$) is the energy and angular momentum of the impacting (scattered) electron, J is the total angular momentum produced by coupling of the target wave function to the continuum angular momentum of the electron and M is the projection of the total angular momentum. It should be noted that, in the case of ionization, the bound electron is replaced by the ejected electron in the final configuration of equation (3). The summation is then performed over all angular momenta of the new wave function and the ejected electron.

The DW approximation often provides higher ionization cross sections compared to measurements for neutral atoms and near neutral ions. The sDW cross sections [10–12] are used here to analyze the ionization process in the oxygen atom.

Study of DI for the ground configuration of the O atom includes $2s$ and $2p$ subshells:

$$[\mathrm{He}]\ 2s^2 2p^4 \ + e^- \rightarrow [\mathrm{He}] \begin{cases} 2s^2 2p^3 \\ 2s 2p^4 \end{cases} + 2e^-. \tag{4}$$

Here, [He] means a He-like electron structure, i. e. $1s$ orbital is fully occupied. The ionization of the $1s$ subshell subsequently leads to states of the O^{2+} ion and, therefore, is not important in the single ionization study.

Excitations from the $2s$ and $2p$ subshells to autoionizing configurations are analyzed for the first step of the EA process:

$$[\mathrm{He}]\ 2s^2 2p^4 \ + e^- \rightarrow [\mathrm{He}] \begin{cases} 2s 2p^4 nl \\ 2s^2 2p^3 nl \end{cases} + e^-, \tag{5}$$

where $n \leqslant 10$, $l \leqslant 4$, $l < n$. The excitations to the higher orbital quantum numbers ($l > 4$) provide a negligible contribution to the single ionization cross sections for the oxygen atom. This study of the EA process includes the outermost subshell of the ground configuration since it was previously demonstrated that these excitations are often important explaining measurements [23–25].

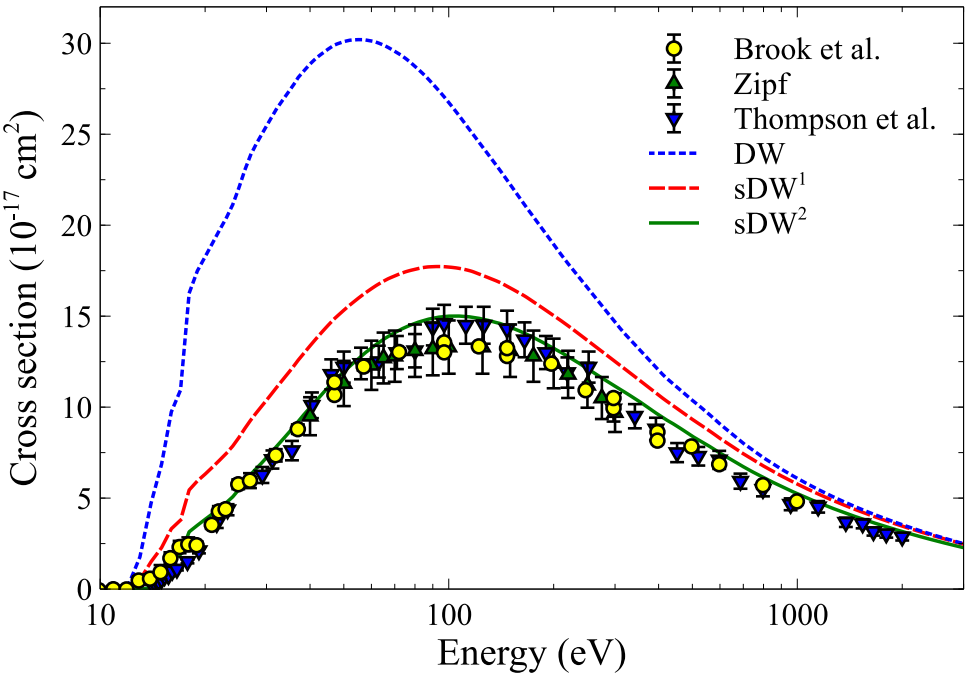

Figure 1. Ionization cross sections for the ground energy level of the O atom. sDW^1 - results obtained using theoretical ionization threshold, sDW^2 - data produced using the NIST ionization threshold. Experiment: Brook *et al* [16], Zipf [17], Thompson *et al* [18].

Table 1. Comparison of theoretical (DFS) and NIST energy levels for the ground $2s^22p^4$ configuration of the O atom.

Index	Term	J	NIST	DFS
0	^3P	2	0.0000	0.0000
1		1	0.0196	0.0170
2		0	0.0281	0.0243
3	^1D	2	1.9674	2.0896
4	^1S	0	4.1897	5.2150

3. Results

Electron-impact single ionization cross sections for energy levels of the ground configuration of the O atom are calculated using the DW approximation (figure 1). This demonstrates that the DW approximation overestimates experimental values [16–18] at peaks approximately by a factor of two for the ground energy level. What is more, the theoretical peak is shifted to the lower energy side by ~40 eV compared to the experimental one. The sDW cross sections show much better agreement with measurements, however, the difference of ~20 % is still obtained in this case. Therefore, the study of the cross sections is extended by incorporating values of the energy levels (table 1) and ionization threshold (13.618 eV) recommended by the National Institute of Standards and Technology (NIST) [26]. In this case, a quite good agreement of the theoretical cross sections with the measurements [16–18] is obtained. It should be noted that there is a discrepancy for the energy levels between the NIST and DFS data (table 1). This can be explained by the correlation effects that are absent when the single configuration method is employed. More elaborate methods are needed to account for correlation effects.

The total ionization cross sections from energy levels of the ground configuration are presented in figure 2 and table 2. Only the $^3P_2$ level is shown for the ^3P term in figure 2 since all three energy levels of the term have the cross sections which are in close agreement with each other. The single ionization cross sections of the $^1D_2$ and $^1S_0$ levels are above the cross sections of the ground energy level by ~10% and ~20% at peaks, respectively. It should be noted that the cross sections corresponding to the ionization from the two highest energy levels of the ground configuration exhibit prominent increases at lower energies of the impacting electron. These structures arise due to excitations from the $2p$ subshell.

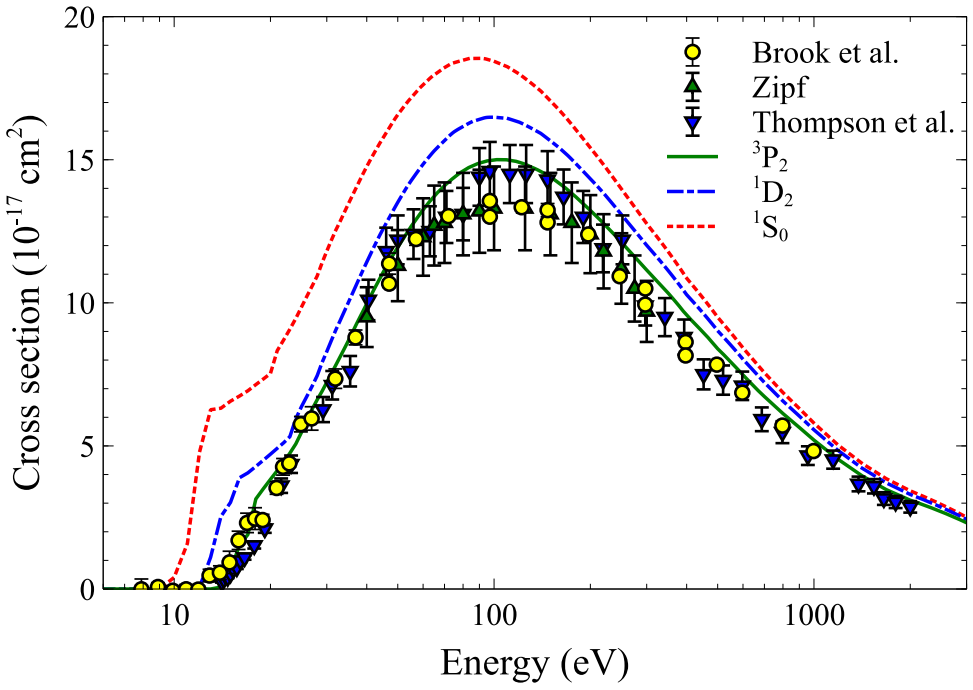

Figure 2. Ionization cross sections for the energy levels of the ground configuration of the O atom. sDW data are produced using the NIST ionization threshold and corresponding energy levels. Experiment: Brook *et al* [16], Zipf [17], Thompson *et al* [18].

Table 2. Electron-impact ionization cross sections (in 10^{-20} cm^2) for energy levels for the ground $2s^2 2p^4$ configuration of the O atom. ε - electron energy in eV, $a \pm b = a \times 10^{\pm b}$.

ε	$^3P_2$	$^3P_1$	$^3P_0$	$^1D_2$	$^1S_0$
9	0.000+0	0.000+0	0.000+0	0.000+0	1.264-1
10	0.000+0	0.000+0	0.000+0	0.000+0	4.061+2
11	0.000+0	0.000+0	0.000+0	0.000+0	1.591+3
12	0.000+0	0.000+0	0.000+0	6.184+1	4.780+3
13	0.000+0	0.000+0	0.000+0	1.109+3	6.265+3
14	6.598+1	6.637+1	6.285+1	2.533+3	6.318+3
15	6.427+2	6.355+2	6.337+2	3.025+3	6.563+3
20	3.831+3	3.904+3	3.974+3	4.711+3	7.532+3
30	7.224+3	7.329+3	7.424+3	8.298+3	1.181+4
50	1.194+4	1.209+4	1.221+4	1.351+4	1.657+4
60	1.325+4	1.340+4	1.353+4	1.484+4	1.762+4
70	1.409+4	1.425+4	1.438+4	1.567+4	1.822+4
80	1.460+4	1.476+4	1.489+4	1.616+4	1.848+4
90	1.488+4	1.504+4	1.518+4	1.641+4	1.854+4
100	1.500+4	1.516+4	1.529+4	1.649+4	1.844+4
110	1.500+4	1.516+4	1.530+4	1.645+4	1.825+4
120	1.491+4	1.507+4	1.520+4	1.631+4	1.799+4
150	1.439+4	1.454+4	1.466+4	1.566+4	1.706+4
200	1.323+4	1.336+4	1.348+4	1.433+4	1.542+4
250	1.212+4	1.223+4	1.234+4	1.309+4	1.398+4
300	1.115+4	1.125+4	1.135+4	1.201+4	1.277+4
350	1.034+4	1.044+4	1.053+4	1.113+4	1.179+4
400	9.565+3	9.658+3	9.739+3	1.028+4	1.086+4
500	8.396+3	8.475+3	8.546+3	9.024+3	9.497+3
700	6.726+3	6.789+3	6.847+3	7.216+3	7.558+3
1000	5.203+3	5.250+3	5.294+3	5.563+3	5.796+3
2000	3.103+3	3.131+3	3.157+3	3.305+3	3.431+3
5000	1.412+3	1.422+3	1.430+3	1.475+3	1.515+3
10000	7.616+2	7.655+2	7.689+2	7.845+2	8.033+2
20000	5.545+2	5.571+2	5.593+2	5.689+2	5.821+2
40000	3.485+2	3.499+2	3.509+2	3.545+2	3.620+2

Table 3. Maximum values of the EA cross sections σ_i (in 10^{-20} cm^2) corresponding to the $2s \rightarrow nl$ ($n \leqslant 10$, $l \leqslant 4$) excitations from the level i of the ground configuration (table 1) to all autoionizing levels of the excited configurations. In addition, minimum and maximum DFS energies (in eV) for levels of configurations produced by the excitations from the 2*s* subshell are presented. Energies are shown relative to the ground energy level. Only the strongest channels ($\sigma_i > 10^{-23}$ cm^2) are presented.

nl	E_{min}	E_{max}	σ_0	σ_1	σ_2	σ_3	σ_4
2p	17.07	25.31	2140.032	2245.709	2348.901	2105.143	2374.804
3s	23.14	35.94	177.716	177.949	177.139	175.527	168.784
3p	24.58	38.09	39.853	40.258	40.656	51.311	49.133
3d	25.97	38.42	6.750	6.759	6.727	6.616	6.381
4s	25.59	38.06	37.960	38.010	37.842	37.566	36.207
4p	26.07	38.76	12.805	12.845	12.847	16.071	15.475
4d	26.70	39.12	3.632	3.637	3.620	3.561	3.437
4f	26.54	38.92	0.042	0.042	0.042	0.041	0.038
5s	26.41	38.82	14.276	14.296	14.230	14.129	13.627
5p	26.57	39.07	5.813	5.821	5.792	7.241	6.959
5d	26.81	39.21	2.044	2.047	2.038	2.007	1.934
5f	26.84	39.23	0.034	0.034	0.034	0.034	0.031
6s	26.78	39.18	6.912	6.921	6.891	6.846	6.605
6p	26.86	39.30	3.108	3.113	3.092	3.694	3.552
6d	26.97	39.36	1.234	1.235	1.230	1.211	1.167
6f	27.01	39.40	0.024	0.024	0.024	0.024	0.022
7s	26.98	39.37	3.873	3.879	3.861	3.835	3.701
7p	27.02	39.43	1.782	1.816	1.757	2.196	2.113
7d	27.08	39.47	0.795	0.796	0.792	0.780	0.752
7f	27.11	39.50	0.017	0.017	0.017	0.017	0.015
8s	27.09	39.48	2.388	2.392	2.380	2.365	2.282
8p	27.12	39.52	1.134	1.137	1.129	1.409	1.357
8d	27.16	39.54	0.540	0.540	0.538	0.530	0.510
8f	27.18	39.56	0.012	0.012	0.012	0.012	0.011
9s	27.16	39.55	1.576	1.579	1.571	1.562	1.507
9p	27.18	39.58	0.771	0.773	0.768	0.957	0.922
9d	27.21	39.59	0.382	0.383	0.381	0.376	0.362
9f	27.22	39.61	0.009	0.009	0.009	0.009	0.008
10s	27.21	39.60	1.095	1.097	1.091	1.085	1.047
10p	27.22	39.62	0.547	0.549	0.546	0.679	0.655
10d	27.24	39.63	0.281	0.281	0.280	0.276	0.265
10f	27.25	39.64	0.006	0.006	0.007	0.007	0.006

Tables 3 and 4 present EA channels corresponding to excitations from the 2*s* and 2*p* subshells, respectively. The strongest excitations to subshells with the same principal quantum number correspond to transitions where the orbital quantum number remains unchanged ($\Delta l = 0$). Previous studies have shown that the excitations up to shells with a principal quantum number $n \approx 20$ must be analyzed to ensure convergence of the EA channels [27, 28]. However, there is no need to take such high excitations into account for the oxygen atom. The $2s \rightarrow 2p$ excitation contributes ~90% to the total EA cross sections from the 2*s* subshell. The second strongest EA channel corresponds to the $2s \rightarrow 3s$ excitation (~5% at peak) (table 3). The strongest EA channel corresponding to the excitations from the 2*p* subshell arises from the transition to the 3*p* subshell (table 4). As it can be seen from tables 3 and 4, the convergence of the EA partial cross sections involving single electron excitations from the 2*p* shell are much slower than those of associated with the single electron excitations from the 2*s* subshell.

The total EA cross sections produced by excitations from the 2*s* subshell are ~50% higher compared to the those from the 2*p* subshell for the energy levels of the ^3P term (tables 3 and 4). On the other hand, the EA cross sections for the excitations from the 2*p* subshell for the $^1D_2$ and $^1S_0$ levels of the ground configuration result in higher peak values by ~30% and ~100%, respectively, compared to the excitations from the 2*s* subshell.

Electron impact ionization cross sections of oxygen atom were previously calculated within the BEB [13], CCO [14], and BSR [15] methods. Our present sDW results along with the previously published results are compared with the measurements [16–18] (without error bars) in figure 3. The BSR-1116 results represent calculations obtained using the close-coupling expansion that includes 1116 states of the oxygen atom. It is interesting that the sDW data show a good agreement with the BEB calculations. The CCO and BSR-1116 data are below the sDW and BEB results at peaks. What is more, the peak of the CCO cross sections is shifted to the lower energy side from the experimental and other theoretical peaks.

The sDW cross sections corresponding to the DI and EA channels are compared to the BSR-1116 calculations [15] for the $^3P_2$, $^1D_2$, and $^1S_0$ energy levels of the ground configuration in figures 4–6. Surprisingly,

Table 4. Maximum values of the EA cross sections σ_i (in 10^{-20} cm^2) corresponding to the $2p \rightarrow nl$ ($n \leqslant 10, l \leqslant 4$) excitations from the level i of the ground configuration (table 1) to all autoionizing levels of the excited configurations. In addition, minimum and maximum DFS energies (in eV) for levels of configurations produced by the excitations from the $2p$ subshell are presented. Energies are shown relative to the ground energy level. Only the strongest channels ($\sigma_i > 10^{-23}$ cm^2) are presented.

nl	E_{min}	E_{max}	σ_0	σ_1	σ_2	σ_3	σ_4
3p	9.50	16.13	586.178	602.211	612.024	877.106	2627.506
3d	10.79	16.08	276.630	273.137	282.566	525.239	569.175
4s	10.39	15.75	18.993	15.026	34.000	45.172	238.339
4p	10.91	16.59	393.602	389.846	400.673	677.741	740.250
4d	11.50	16.79	131.472	129.969	134.239	245.924	265.710
4f	11.35	16.61	2.124	2.177	2.289	4.805	6.423
5s	11.21	16.51	33.781	32.915	41.334	83.154	77.521
5p	11.38	16.82	162.448	160.905	165.524	287.966	317.165
5d	11.65	16.93	70.298	69.394	71.972	132.141	142.255
5f	11.65	16.92	1.721	1.749	1.828	3.874	5.170
5g	11.65	16.91	0.023	0.026	0.028	0.065	0.083
6s	11.59	16.86	15.820	15.230	18.595	37.736	34.221
6p	11.67	17.02	83.102	82.305	84.687	148.789	164.453
6d	11.78	17.05	41.476	40.754	42.347	77.791	83.929
6f	11.82	17.08	1.166	1.206	1.270	2.644	3.613
6g	11.82	17.08	0.026	0.032	0.036	0.075	0.103
7s	11.78	17.05	8.917	8.457	10.050	20.460	18.295
7p	11.83	17.14	47.315	47.156	48.868	84.944	96.148
7d	11.89	17.16	26.267	25.729	26.818	49.139	53.010
7f	11.92	17.18	0.777	0.815	0.865	1.788	2.515
7g	11.92	17.18	0.021	0.037	0.042	0.067	0.093
8s	11.90	17.16	5.543	5.204	6.076	12.382	10.993
8p	11.92	17.22	29.990	29.676	30.529	53.748	60.342
8d	11.96	17.23	17.648	17.210	18.018	32.959	35.548
8f	11.98	17.25	0.552	0.567	0.603	1.254	1.718
8g	11.98	17.25	0.016	0.019	0.021	0.045	0.071
9s	11.97	17.24	3.681	3.434	3.964	8.079	7.145
9p	11.99	17.27	20.223	20.001	20.572	36.286	39.795
9d	12.01	17.28	12.416	12.029	12.677	23.162	24.974
9f	12.03	17.29	0.405	0.416	0.436	0.909	1.225
9g	12.03	17.29	0.013	0.015	0.016	0.034	0.054
10s	12.02	17.28	2.569	2.385	2.733	5.571	4.917
10p	12.03	17.31	14.301	14.133	14.530	25.666	28.178
10d	12.05	17.32	9.065	8.776	9.252	16.898	18.219
10f	12.06	17.32	0.304	0.312	0.327	0.677	0.898
10g	12.06	17.32	0.010	0.012	0.013	0.027	0.043

the DI $2s$ and DI $2p$ channels show a good agreement with the BSR-1116 data for the $^3P_2$ and $^1D_2$ energy levels at peaks. For the highest energy level (figure 6), the sDW DI $2p$ channel is below the BSR-1116 calculations by ∼15% at the peak. What is interesting, the cross sections from BSR show a strong increase starting at ∼11 eV, while the sDW data appear at ∼15 eV. Therefore, the sDW cross sections corresponding to transitions from the $^1S_0$ level to the levels ($^4S_{3/2}$, $^2D_{5/2,3/2}$, $^2P_{1/2,3/2}$) of the $2p^3$ configuration are analyzed in more detail. The cross sections from the $^1S_0$ level to the levels of the $2p^3$ configuration differ by six orders of magnitude. The weakest transition (∼10^{-23} cm^2) occurs to the $^4S_{3/2}$ energy level, which is the lowest one, of the $2p^3$ configuration. There is no $^1S_0 \rightarrow {}^2D_{5/2}$ transition presented in the output of FAC. The cross sections at peak for $^1S_0 \rightarrow {}^2D_{3/2}$ reach over $\sim 4 \cdot 10^{-21}$ cm^2. The $^1S_0 \rightarrow {}^2P_{1/2,3/2}$ transitions with threshold of ∼15 eV are the strongest ones for the DI $2p$ channel (∼10^{-17} cm^2). Therefore, it can be deduced that the BSR-1116 ionization cross sections from the $^1S_0$ level to the lowest levels of the $2p^3$ configuration are much stronger compared to the sDW data. The reason why DI cross section of the [He] $2p^3$ ($^3P_2$) level calculated by the BSR is larger than our sDW results over a large energy range starting from the threshold is not clear.

It should be noted that the BSR-1116 data show a similar contribution from the EA process to the total ionization cross sections at peaks ($\sim 2 \cdot 10^{-17}$ cm^2) for all levels of the ground configuration (figures 4–6). The contributions from the indirect process to the total cross sections of the levels $^3P_2$, $^1D_2$, and $^1S_0$ within the sDW approximation at the peak energies are $\sim 3 \cdot 10^{-17}$ cm^2, $\sim 4 \cdot 10^{-17}$ cm^2, and $\sim 5 \cdot 10s^{-17}$ cm^2, respectively. Higher contributions of the EA channels for the higher levels compared to the lower levels of the ground configuration were also obtained for other ions using the sDW approximation [12, 25]. Reason for the disagreement between

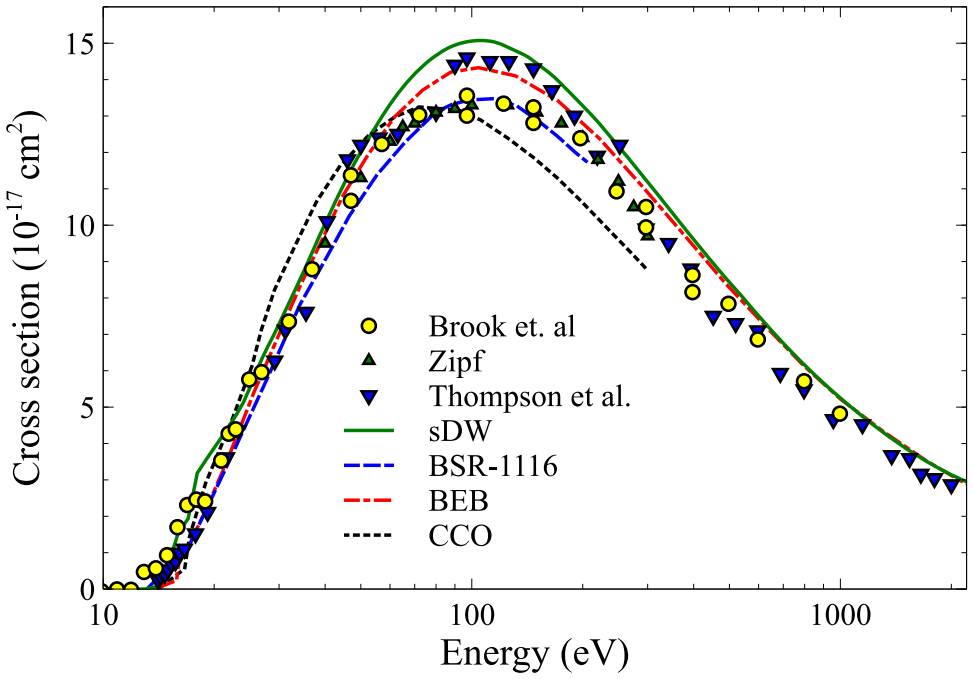

Figure 3. Ionization cross sections for the ground energy level of the O atom. sDW data are produced using the NIST ionization threshold. Experiment: Brook *et al* [16], Zipf [17], Thompson *et al* [18].

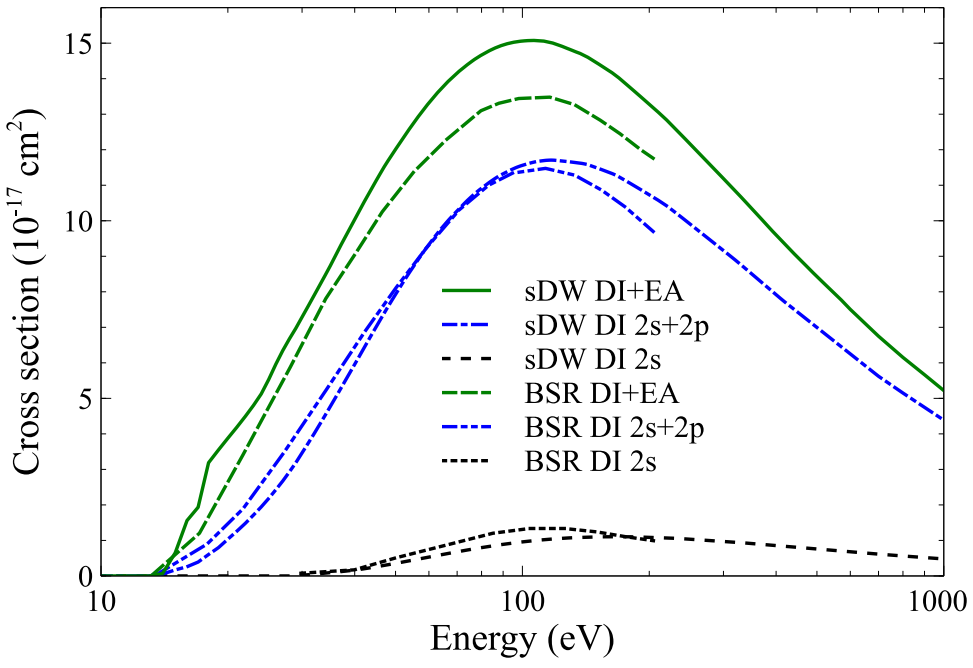

Figure 4. DI and EA cross sections for the ground energy level of the O atom. The sDW data are produced using the NIST ionization threshold. BSR corresponds to BSR-1116 results [15].

the BSR-1116 and sDW results can be attributed to the correlation effects that are missing in the current work. The BSR-1116 calculations include inner-core or short-range correlation effects by considering configuration interaction expansions for the $2s^22p^3$ and $2s2p^4$ ionic states. These expansions involve all single and double excitations from the $2s$ and $2p$ orbitals to the $3l$ and $4l$ ($l = 0 - 3$) correlated orbitals [15]. However, additional studies using different methods are needed to resolve this issue.

The shoulder-like structures seen on the lower energy side of our total sDW ionization cross sections (figure 2) are not seen in the BSR results. These structures are formed by excitations from the $2p$ subshell and is

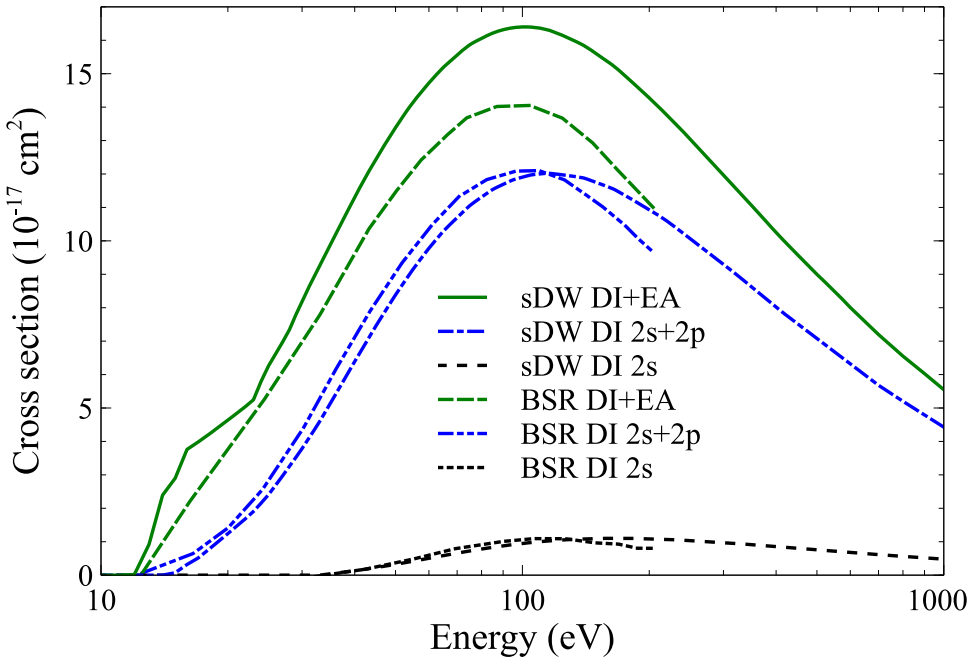

Figure 5. DI and EA cross sections for the $^1D_2$ level of the O atom. The sDW data are produced using energy level and ionization threshold from NIST. BSR corresponds to BSR-1116 [15].

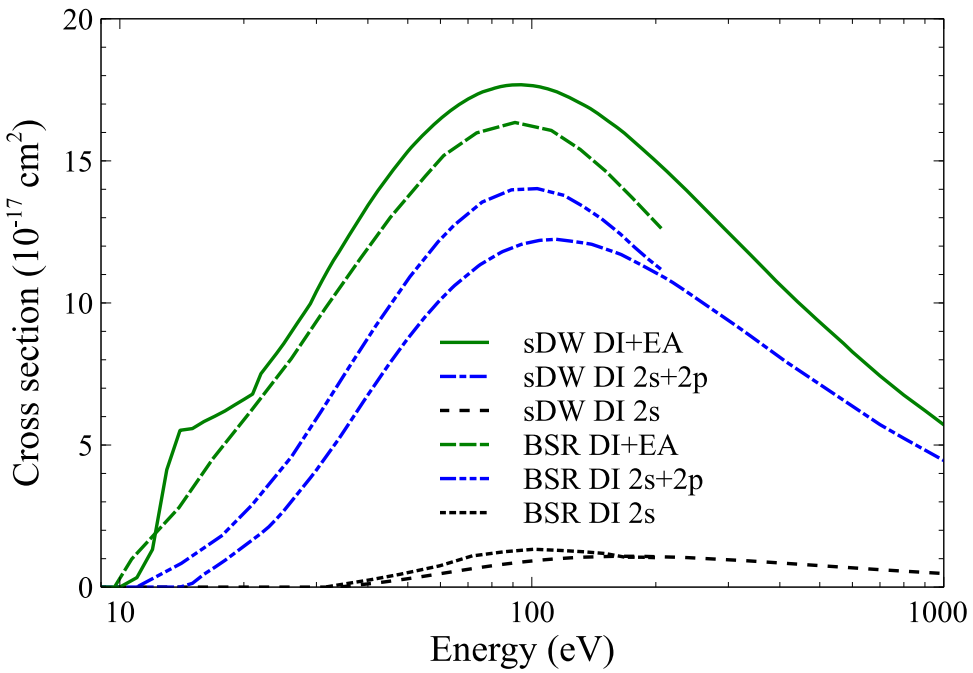

Figure 6. DI and EA cross sections for the $^1S_0$ level of the O atom. The sDW data are produced using energy level and ionization threshold from NIST. BSR corresponds to BSR-1116 [15].

more prominent for the highest energy level of the ground configuration. The EA 2*s* and EA 2*p* channels for the $^1S_0$ level of the ground configuration are compared in figure 7. The form of the cross sections shows that the main contribution to the EA 2*p* channel comes from the forbidden transitions. Therefore, to understand a reason for the disagreement with the BSR calculations, the sDW and BSR excitation cross sections are compared for transitions that are forbidden by the spin selection rule, which were analyzed previously [15]. The cross sections for the $2p^4\ ^3P \rightarrow 2p^3 3s\ ^5S$ excitation are presented in figure 8. It can be seen that the sDW results are in good agreement with the BSR-1116 calculations, except for the resonance structure. For the $2p^4\ ^3P \rightarrow 2p^3 3p\ ^5P$ excitation (figure 9), the BSR-1116 cross sections are about twice as large as the sDW data at ~ 50 eV. However,

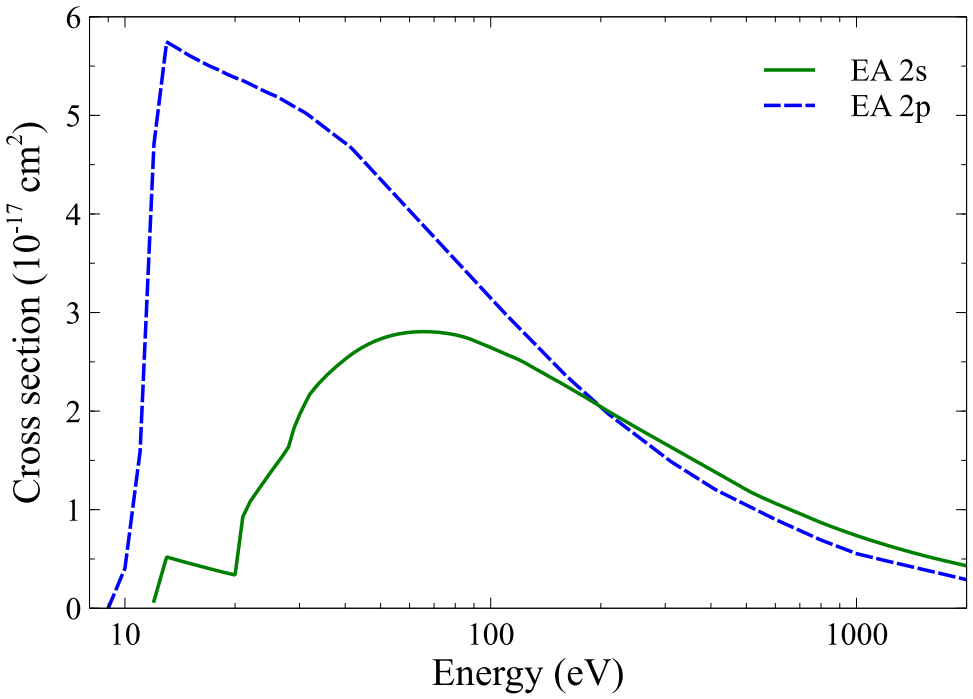

Figure 7. EA 2*s* and EA 2*p* channels for the $^1S_0$ level.

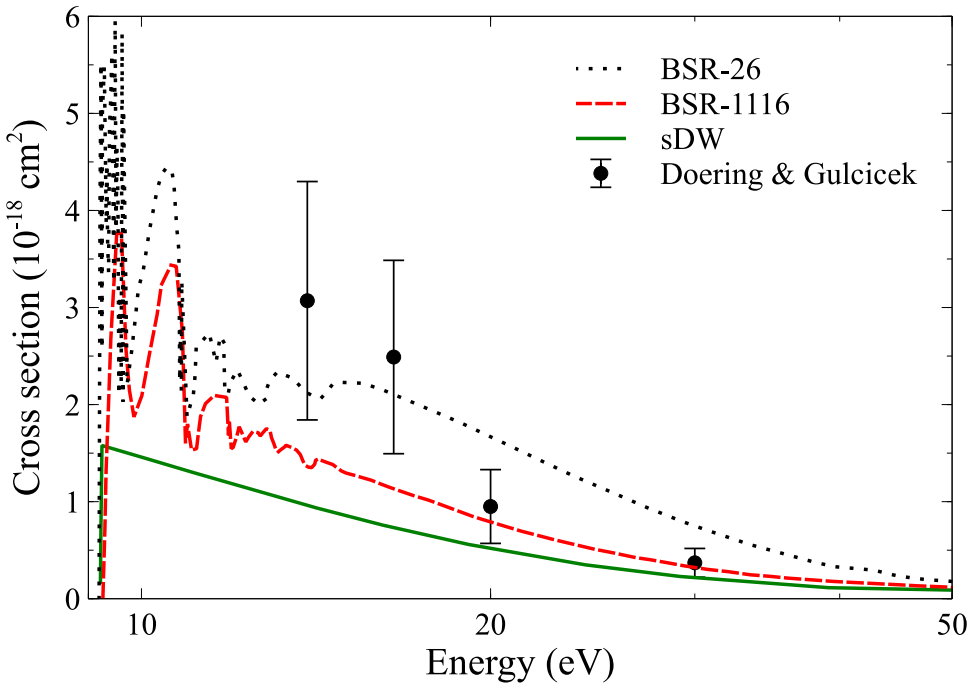

Figure 8. Excitation cross sections for $2p^4\ ^3P \rightarrow 2p^3 3s\ ^5S$ transition. BSR-26 results are from [29], BSR-1116—[15], experimental data—Doering and Gulcicek [30].

the trend of the decrease with increasing energy is very similar for both calculations in this transition. It should be noted that the DW approximation yields cross sections significantly higher than the BSR-1116 data at the excitation threshold (figure 9). Moreover, the DW cross sections intersect the BSR-1116 cross sections at approximately 20 eV. So, the sDW results for the spin-forbidden transitions are slightly lower than the BSR data (figures 8 and 9). Apparently, these structures (figure 2) are wiped out by the inclusion of the resonance excitations in BSR calculations which are missing from our calculations.

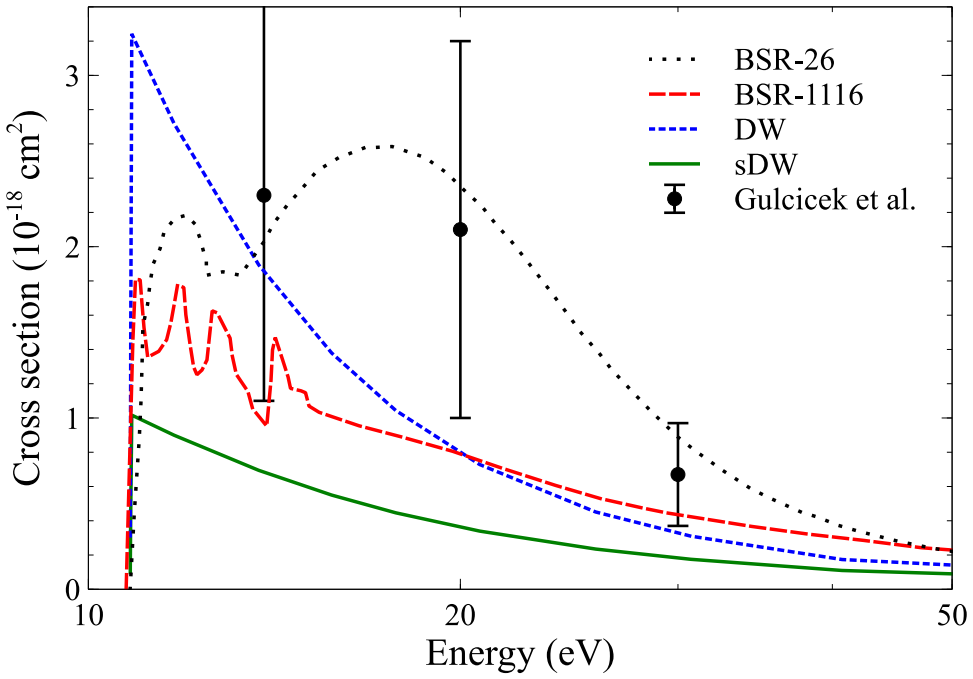

Figure 9. Excitation cross sections for $2p^4\ ^3P \rightarrow 2p^3 3p\ ^5P$ transition. The present sDW and DW results are compared to the BSR-26 [29], BSR-1116 [15], and experimental data [31].

4. Summary and conclusions

Electron-impact ionization for energy levels of the ground configuration of the O atom is investigated using the DW approximation with scaling functions. The DW cross sections overestimate measurements approximately by a factor of two at peak values. The sDW cross sections obtained using the ionization threshold provided by NIST show a good agreement with experimental data for the ground energy level. The sDW cross sections are ~4% higher than BEB data at peak and ~10% higher than the BSR results.

Comparison of DI channels corresponding to the sDW and BSR calculations show a good agreements at peak values for the ionization from the ^3P and ^1D terms of the ground configuration. However, the BSR approach provides ~15% larger contribution compared to the sDW results for the $^1S_0$ level. The reason of the discrepancy is not clear. What is more, the EA contribution at peaks of the total ionization cross sections for the BSR-1116 calculations is similar for all three terms of the ground configuration while higher energy levels show the higher contribution from the indirect ionization process for the sDW data.

It should be noted that the $2s \rightarrow 2p$ excitation provides main contribution to the EA process corresponding to the excitations from the $2s$ subshell. There is seen the shoulder-like structures in the sDW cross sections at low-energy side for $^1D_2$ and $^1S_0$ levels. These structures arises from the forbidden transitions. The BSR approach does not provide any structures of the cross sections at lower energies of impacting electron. Apparently, these structures are wiped out in the BSR calculations due to resonance excitations absent from our calculations.

Finally, the sDW cross sections for the spin forbidden transitions $2p^4\ ^3P \rightarrow 2p^3 3s\ ^5S$ and $2p^4\ ^3P \rightarrow 2p^3 3p\ ^5P$ show quite good agreement with the BSR-1116 calculations (except in the resonance region). The DW approximation provides results that are significantly higher than the BSR-1116 data at peaks.

Acknowledgments

Part of the computations were performed on the High Performance Computing (HPC) cluster at the Institute of Theoretical Physics and Astronomy, Faculty of Physics, Vilnius University.

Data availability statement

All data that support the findings of this study are included within the article (and any supplementary files).

ORCID iDs

V Jonauskas https://orcid.org/0000-0002-5035-6270

References

[1] Cescutti G, Matteucci F, McWilliam A and Chiappini C 2009 *Astron. Astrophys.* **505** 605–12
[2] Pérez-Montero E *et al* 2013 *Astron. Astrophys.* **549** A25
[3] Dupree A K, Avrett E H and Kurucz R L 2016 *Astrophys. J. Lett.* **821** L7
[4] Zinchenko I A, Vílchez J M, Pérez-Montero E, Sukhorukov A V, Sobolenko M and Duarte Puertas S 2021 *Astron. Astrophys.* **655** A58
[5] Laseter I H *et al* 2024 *Astron. Astrophys.* **681** A70
[6] Tendler M, Neuhauser J and Wunderlich R 1984 *Nucl. Fusion* **24** 989
[7] Henderson S S *et al* 2018 *Nucl. Fusion* **58** 016047
[8] He D, Liu Y, Zhao T, Zhu J and Yu G 2008 *J. Nanopart. Res.* **10** 409–14
[9] Li H, Singh A, Bayram F, Childress A S, Rao A M and Koley G 2019 *Nanoscale* **11** 11145–51
[10] Jonauskas V 2018 *Astron. Astrophys.* **620** A188
[11] Kynienė A, Kučas S, Pakalka S, Masys Š and Jonauskas V 2019 *Phys. Rev. A* **100** 052705
[12] Jonauskas V 2020 *At. Data Nucl. Data Tables* **135-136** 101363
[13] Kim Y-K and Desclaux J-P 2002 *Phys. Rev. A* **66** 012708
[14] Wang Y and Zhou Y 2006 *J. Phys. B* **39** 3009
[15] Tayal S S and Zatsarinny O 2016 *Phys. Rev. A* **94** 042707
[16] Brook E, Harrison M F A and Smith A C H 1978 *J. Phys. B* **11** 3115–32
[17] Zipf E C 1985 *Planet. Space Sci.* **33** 1303–7
[18] Thompson W R, Shah M B and Gilbody H B 1995 *J. Phys. B* **28** 1321
[19] Fite W L and Brackmann R T 1959 *Phys. Rev.* **113** 815–6
[20] Rothe E W, Marino L L, Neynaber R H and Trujillo S M 1962 *Phys. Rev.* **125** 582–3
[21] Gu M F 2008 *Can. J. Phys.* **86** 675–89
[22] Zatsarinny O and Bartschat K 2014 *J. Phys. B* **47** 061001
[23] Kwon D-H and Savin D W 2012 *Phys. Rev. A* **86** 022701
[24] Kynienė A and Jonauskas V 2021 *Astron. Astrophys.* **656** A79
[25] Jonauskas V 2022 *Astron. Astrophys.* **659** A11
[26] Kramida A, Ralchenko Y, Reader J and NIST ASD Team 2024 *NIST Atomic Spectra Database (version 5.12)* (National Institute of Standards and Technology) [accessed 14 February 2025] (https://doi.org/10.18434/T4W30F)
[27] Kynienė A, Masys Š and Jonauskas V 2015 *Phys. Rev. A* **91** 062707
[28] Kynienė A, Pakalka S, Masys Š and Jonauskas V 2016 *J. Phys. B* **49** 185001
[29] Zatsarinny O and Tayal S S 2001 *J. Phys. B* **34** 1299
[30] Doering J P and Gulcicek E E 1989 *J. Geophys. Res.: Space Phys* **94** 2733–6
[31] Gulcicek E E, Doering J P and Vaughan S O 1988 *J. Geophys. Res.: Space Phys* **93** 5885–9